

# Large-area broadband saturable Bragg reflectors by use of oxidized AlAs

S. N. Tandon, J. T. Gopinath, H. M. Shen, G. S. Petrich, L. A. Kolodziejski, F. X. Kärtner, and E. P. Ippen

Research Laboratory of Electronics, Massachusetts Institute of Technology, Cambridge, Massachusetts 02139

Received June 16, 2004

Broadband saturable Bragg reflectors (SBRs) are designed and fabricated by monolithic integration of semiconductor saturable absorbers with broadband Bragg mirrors. The wet oxidation of AlAs creates low-index  $\text{Al}_x\text{O}_y$  layers for broadband, high-index-contrast  $\text{AlGaAs}/\text{Al}_x\text{O}_y$  or  $\text{InGaAlP}/\text{Al}_x\text{O}_y$  mirrors. SBR mirror designs indicate greater than 99% reflectivity over bandwidths of 294, 466, and 563 nm for center wavelengths of 800, 1300, and 1550 nm, respectively. Highly strained and unstrained absorbers are stably integrated with the oxidized mirrors. Large-scale lateral oxidation techniques permit the fabrication of SBRs with diameters of 500  $\mu\text{m}$ . Large-area, broadband SBRs are used to self-start and mode lock a variety of laser systems at wavelengths from 800 to 1550 nm. © 2004 Optical Society of America

OCIS codes: 140.4050, 160.6000, 230.1480, 320.7090.

Semiconductor saturable absorber mirrors can be used for pulse generation in a variety of solid-state and fiber lasers. Saturable absorber mirrors can be employed either as the primary mode-locking element in these lasers or as a starting mechanism for other mode-locking techniques, such as Kerr lens mode locking. With an absorber to initiate pulsing, the critical cavity alignment otherwise required for Kerr lens mode locking is relaxed.<sup>1</sup> In addition, the absorber can stabilize lasers against environmental fluctuations. Semiconductor saturable absorbers can be integrated with a mirror with a variety of approaches, including monolithic integration of absorbers with Bragg mirrors and integration of absorbers with metal mirrors by use of postprocessing methods. Through epitaxial growth, absorbers have been monolithically integrated with GaAs/AlAs ( $n \sim 3.4/2.9$ )<sup>2,3</sup> or AlGaAs/AlAs Bragg mirrors.<sup>4–6</sup> However, the low index contrast (maximum  $\Delta n \sim 0.5$ ) results in narrow-bandwidth mirrors, which limits the pulse widths generated. A broadband epitaxially grown AlGaAs/ $\text{CaF}_2$  mirror was monolithically integrated with a GaAs absorber for use in a Ti:sapphire laser.<sup>7</sup> However, because AlGaAs and  $\text{CaF}_2$  have different material characteristics (e.g., thermal, structural), the epitaxial growth of the layered structure is challenging. Absorbers have also been transferred to broad-bandwidth metal mirrors by use of postgrowth processing methods.<sup>8,9</sup> Although metallic mirrors introduce greater losses than Bragg mirrors, additional dielectric layers have helped reduce the effective losses.

In this Letter an alternative approach is described to monolithically integrate semiconductor absorbers onto low-loss, broadband, Bragg mirrors, creating broadband saturable Bragg reflectors (SBRs). After the absorber layer is epitaxially grown on nominally lattice-matched, low-index-contrast AlGaAs/AlAs or InGaAlP/AlAs dielectric stacks, steam oxidation is used to convert the AlAs ( $n \sim 2.9$ ) layers into lower-index  $\text{Al}_x\text{O}_y$  ( $n \sim 1.6$ ) layers. The lateral oxidation lengths achieved here (hundreds of micrometers) are much larger than the length scales used most commonly in vertical-cavity surface-emitting laser fabrication (tens of micrometers).<sup>10</sup> The result is

an absorber integrated directly with a high-index-contrast mirror with  $\Delta n$  greater than 1.5. Varying the material composition allows the absorber bandgap to be engineered to match the operating wavelength of the laser. A controlled oxidation technique also allows highly strained absorbers to be successfully integrated into SBRs without degradation of the structure. As a result, broadband SBRs are successfully engineered for a variety of absorption characteristics, with mirror reflectivities ranging from 750 to 1850 nm.

A schematic of the broadband SBR is shown in Fig. 1. The device consists of a half-wave layer composed of an absorbing layer between two cladding layers on a Bragg mirror with alternating quarter-wave layers of high- and low-refractive-index material. Each SBR consists of a 500- $\mu\text{m}$ -diameter circular mesa, which allows great flexibility in the laser spot size. Larger spot sizes ( $>100 \mu\text{m}$ ) are desirable for avoiding the effects of two-photon absorption by allowing a lower energy density. Two-photon absorption can limit the pulse width and may result in pulse breakup.<sup>11,12</sup>

The SBRs described in this Letter have a high-index layer of either  $\text{Al}_{0.3}\text{Ga}_{0.7}\text{As}$  ( $n \sim 3.3$ ) or  $\text{In}_{0.15}\text{Ga}_{0.15}\text{Al}_{0.35}\text{P}$  ( $n \sim 3.1$ ), which are both effectively lattice matched to the GaAs substrate. The low-index layer consists of  $\text{Al}_x\text{O}_y$  ( $n \sim 1.6$ ) resulting from the thermal oxidation of AlAs. The absorber layer can be created with quantum dots, quantum wells, or thick semiconductor layers—the choice depends on the amount of intensity-dependent loss desired in the laser system. The material composition of the absorbing layer is designed to match the laser's operating wavelength.  $\text{In}_x\text{Ga}_{1-x}\text{As}$  absorbing

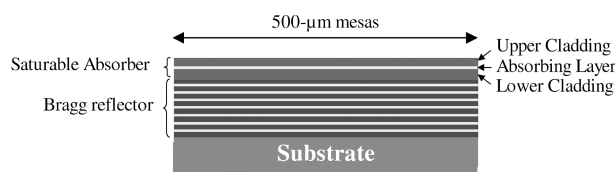


Fig. 1. Schematic of a saturable Bragg reflector highlighting elements of device design.

layers of varying composition were used for the SBRs described here. As the indium content increases, the lattice mismatch introduces strain into the layered structure. Because the SBR is an absorbing rather than an emitting device, higher misfit dislocation densities and higher nonradiative recombination rates due to lattice mismatch can be tolerated and are even desirable for faster recovery times. The material composition of the cladding layers is designed to distribute strain throughout the absorber, thus influencing SBR recovery times. For example, the strain of an  $\text{In}_{0.5}\text{Ga}_{0.5}\text{As}$  absorber grown on GaAs can be distributed away from the absorber interface by use of InP cladding layers. Using GaAs cladding layers instead concentrates strain at the absorber interface. To determine the placement of the absorber within the cladding layers, the standing waves that develop in the SBR are considered. Shifting the position of the absorber within the standing-wave pattern not only affects the SBR's saturation fluence but also alters the wavelength dependence of the saturable absorption. Thus absorber position determines the wavelength range over which the laser is SBR mode locked.

SBR layers are grown with gas-source molecular-beam epitaxy on GaAs substrates. Mesas are defined with photolithography and wet etchants to expose the cross section of the SBR structure for oxidation. A (1:8:40)  $\text{H}_2\text{SO}_4\text{:H}_2\text{O}_2\text{:H}_2\text{O}$  etch is used for arsenic-based SBRs and a (1:1:2)  $\text{HCl:H}_2\text{NO}_3\text{:H}_2\text{O}$  solution is used for InP or InGaAlP layers. Exposed AIAs layers are then laterally oxidized by use of water vapor in a tube furnace. A controlled temperature ramp begins and ends the oxidation process at 100 °C. Typical oxidation temperatures range from 400 °C to 435 °C. To examine the extent of oxidation, cross-sectional images were obtained with scanning electron microscopy (SEM). Reflectivity measurements were obtained with Fourier-transform infrared (FTIR) spectroscopy and a microspectrophotometer. Preoxidation thicknesses were determined from high-resolution x-ray diffraction rocking curves of the as-grown SBRs and FTIR spectroscopy.

The top and cross-sectional views of two SBR designs are shown in Fig. 2. Figures 2(a) and 2(b) show a SBR design for a Cr:forsterite laser system (1300 nm) to generate 30-fs pulses.<sup>13</sup> The top view in Fig. 2(a) shows the fully oxidized 500- $\mu\text{m}$  mesa. The SBR cross section [Fig. 2(b)] shows a 40-nm-thick  $\text{In}_{0.5}\text{Ga}_{0.5}\text{As}$  absorber with 67-nm-thick GaAs cladding layers on top of a 7 $\frac{1}{2}$ -pair  $\text{Al}_{0.3}\text{Ga}_{0.7}\text{As}/\text{Al}_x\text{O}_y$  mirror stack (92 nm/  $\sim 180$  nm). Using  $\text{Al}_{0.3}\text{Ga}_{0.7}\text{As}$  instead of GaAs as the mirror's high-index layer strengthens the bonding between mirror layers upon oxidation while preventing significant oxidation due to its low aluminum content.<sup>10</sup> At an oxidation temperature of 420 °C the AIAs layers in the 500- $\mu\text{m}$ -diameter mirror stack were completely oxidized in 4 h without degradation of the structure. Although oxidation rates increase with temperature, at higher temperatures oxidation of the structure was limited by the delamination of the strained absorber layer. As expected, this delamination effect is more pronounced for thicker

strained absorbers. Slowly ramping the temperature from 100 °C to the oxidation temperature before the oxidation process reduced delamination effects dramatically. With this oxidation process SBR structures with highly strained 100-nm InGaAs absorbers were successfully fabricated. Figures 2(c) and 2(d) show a SBR design for a Ti:sapphire laser (800 nm). The 500- $\mu\text{m}$  mesas [Fig. 2(c)] are not circular due to the  $\text{HCl:H}_2\text{NO}_3\text{:H}_2\text{O}$  wet etch. A 10-nm GaAs absorber with 60-nm  $\text{In}_{0.15}\text{Ga}_{0.15}\text{Al}_{0.35}\text{P}$  layers was integrated with a seven-pair InGaAlP/ $\text{Al}_x\text{O}_y$  (60 nm/  $\sim 135$  nm) mirror.  $\text{In}_{0.15}\text{Ga}_{0.15}\text{Al}_{0.35}\text{P}$ , with a bandgap at 536 nm and refractive index of  $\sim 3.1$ , is lattice matched to GaAs and has a lower absorption wavelength than AlGaAs alloys. With an InGaAlP-based layered structure the SBR design is nominally unstrained. AIAs layers are completely oxidized at 435 °C in 2.5 h with no observable delamination. As seen in both broadband SBR designs, the oxidized AIAs layer is polycrystalline, whereas the high-index semiconductor layer remains single crystal.

With a properly engineered layered structure and controlled large-scale oxidation, SBRs are fabricated with broadband reflectivities from 750 to 1850 nm. Figure 3 presents SBR reflectivity measurements for three different laser systems: Ti:sapphire (800 nm), Cr:Forsterite (1300 nm), and Er: $\text{Bi}_2\text{O}_3$  (1550 nm).<sup>14</sup> Theoretical mirror reflectivities are greater than 99% over bandwidths of 294, 466, and 563 nm, respectively. The Ti:sapphire SBR reflectivity was measured with a microspectrophotometer, whereas reflectivities for the Cr:forsterite and Er: $\text{Bi}_2\text{O}_3$  SBRs were measured with a FTIR spectrometer. All the measurements reveal absorption losses originating from the SBR's absorber layer.

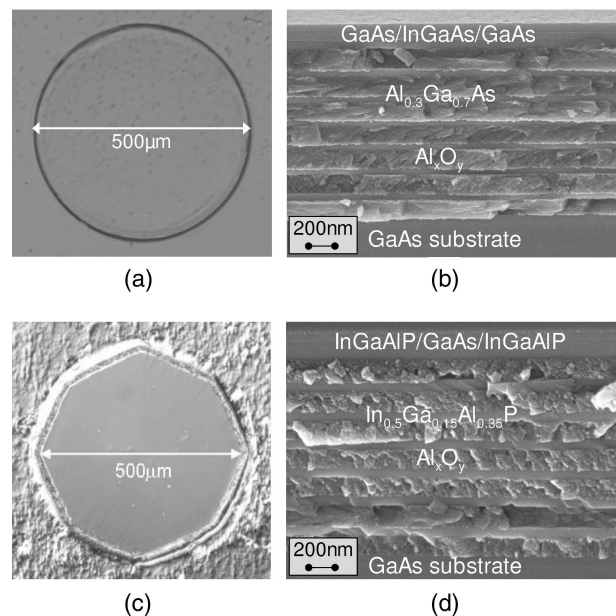


Fig. 2. (a) Differential interference contrast image of a fully oxidized Cr:forsterite SBR. (b) SEM image of the SBR cross section shown in Fig. 2(a). (c) Differential interference contrast image of a fully oxidized Ti:sapphire SBR. (d) SEM image of the SBR cross section shown in Fig. 2(c).

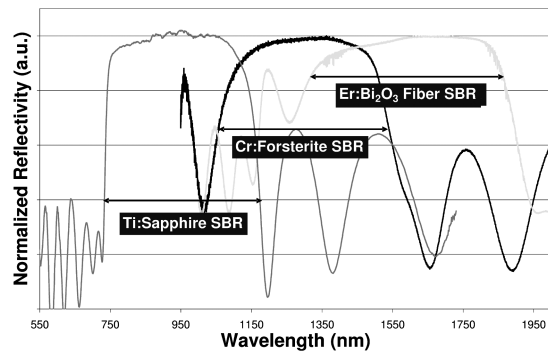


Fig. 3. Reflectivity measurements of SBRs fabricated for three different laser systems: Ti:sapphire, Cr:forsterite, and Er:Bi<sub>2</sub>O<sub>3</sub> fiber.

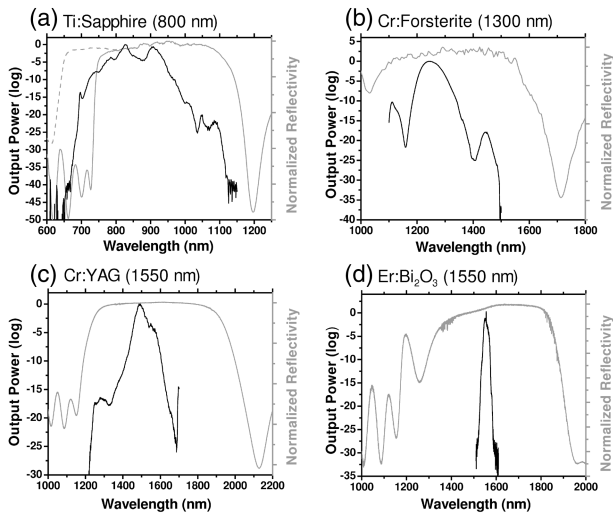


Fig. 4. SBR mode-locked spectra of (a) Ti:sapphire, (b) Cr:forsterite, (c) Cr:YAG, and (d) Er:Bi<sub>2</sub>O<sub>3</sub> lasers with respective SBR reflectivities. In (a) reflectivities of two SBRs from the same wafer are shown. One measurement (dotted curve) was limited in range by the spectrometer used.

Measurements of SBR characteristics were performed. SBRs designed for a Cr:YAG laser (1550 nm) have a saturation fluence of  $\sim 10 \mu\text{J}/\text{cm}^2$ , nonsaturable loss of  $< 0.8\%$ , and modulation depth of 0.3%. SBRs for an Er:Bi<sub>2</sub>O<sub>3</sub> laser have a saturation fluence of  $\sim 10 \mu\text{J}/\text{cm}^2$  and modulation depth of 3%. Ti:sapphire SBRs have a nonsaturable loss of  $< 2\%$ . Figure 4 presents SBR mode-locked spectra of the Ti:sapphire [Fig. 4(a)], Cr:forsterite [Fig. 4(b)], Cr:YAG [Fig. 4(c)], and Er:Bi<sub>2</sub>O<sub>3</sub> [Fig. 4(d)] lasers with their SBR reflectivities. In Fig. 4(a) reflectivities of two representative SBRs from the same wafer are shown. Thickness variation across the wafer resulted in center wavelength differences between SBRs. The Fourier limit implies pulse widths of 15–30 fs for the Ti:sapphire and 20 fs for the Cr:forsterite laser. Autocorrelation measurements reveal pulse widths of 32 and 155 fs for the Cr:YAG and Er:Bi<sub>2</sub>O<sub>3</sub> lasers, respectively. All the SBRs tested produced self-started mode locking that could be sustained for several days

without observable absorber degradation, illustrating the SBR's durability and high damage threshold.

In conclusion, broadband SBRs have been designed and fabricated by use of the large-scale oxidation of AlAs layers monolithically integrated with other III–V layers to form an absorber with a high-index-contrast mirror. A number of characteristics must be considered when designing a layered structure. Absorber layers are chosen based on the absorption wavelength, amount of loss, and desired recovery times. Mirror layers are chosen based on the center wavelength of the laser and the ability to withstand the AlAs oxidation process. The SBRs described here have been used in laser systems from 800 to 1550 nm.

The authors thank Randy Geels of Filmetrics, Inc., for reflectivity measurements with the F10-EXR microspectrophotometer. Many thanks to Thomas Schibli, Richard Ell, Jason Sickler, and Jungwon Kim, who motivated this work by using broadband SBRs in their lasers. This work was funded by Office of Naval Research award N00014-02-1-0717 and made use of Shared Experimental Facilities supported in part by the Materials Research Science and Engineering Center of the National Science Foundation under award DMR 02-13282.

## References

1. R. Fluck, I. D. Jung, G. Zhang, F. X. Kärtner, and U. Keller, *Opt. Lett.* **21**, 743 (1996).
2. U. Keller, D. A. B. Miller, G. D. Boyd, T. H. Chiu, J. F. Ferguson, and M. T. Asom, *Opt. Lett.* **17**, 505 (1992).
3. Y. Chang, R. Maciejko, R. Leonelli, and A. S. Thorpe, *Appl. Phys. Lett.* **73**, 2098 (1998).
4. S. Tsuda, W. H. Knox, E. A. deSouza, W. Y. Jan, and J. E. Cunningham, *Opt. Lett.* **20**, 1406 (1995).
5. J. Shieh, T. C. Huang, K. F. Huang, C. Wang, and C. Pan, *Opt. Commun.* **156**, 53 (1998).
6. S. J. White, J. M. Hopkins, W. H. Knox, and A. Miller, *IEEE J. Quantum Electron.* **38**, 246 (2002).
7. S. Schön, M. Haiml, L. Gallmann, and U. Keller, *Opt. Lett.* **27**, 1845 (2002).
8. D. H. Sutter, G. Steinmeyer, L. Gallmann, N. Matuschek, F. Morier-Genoud, U. Keller, V. Scheuer, G. Angelow, and T. Tschudi, *Opt. Lett.* **24**, 631 (1999).
9. Z. Zhang, T. Nakagawa, K. Torizuka, T. Sugaya, and K. Kobayashi, *Appl. Phys. B* **70**, S59 (2000).
10. S. N. Tandon, J. T. Gopinath, A. A. Erchak, G. S. Petrich, L. A. Kolodziejski, and E. P. Ippen, *J. Electron. Mater.* **33**, 774 (2004).
11. D. J. Ripin, J. T. Gopinath, H. M. Shen, A. A. Erchak, G. S. Petrich, L. A. Kolodziejski, F. X. Kärtner, and E. P. Ippen, *Opt. Commun.* **214**, 285 (2002).
12. E. R. Thoen, E. M. Koontz, M. Joschko, P. Langlois, T. R. Schibli, F. X. Kärtner, E. P. Ippen, and L. A. Kolodziejski, *Appl. Phys. Lett.* **74**, 3927 (1999).
13. T. R. Schibli, J. Kim, O. Kuzucu, J. T. Gopinath, S. N. Tandon, G. S. Petrich, L. A. Kolodziejski, J. G. Fujimoto, E. P. Ippen, and F. X. Kärtner, *Opt. Lett.* **28**, 947 (2003).
14. J. W. Sickler, J. T. Gopinath, S. N. Tandon, H. Sotobayashi, G. S. Petrich, E. P. Ippen, and L. A. Kolodziejski, in *Conference on Lasers and Electro-Optics (CLEO)*, Postconference Digest, Vol. 96 of OSA Trends in Optics and Photonics Series (Optical Society of America, Washington, D.C., 2004), paper CThK6.